

On the evolution of young radio-loud AGN

I.A.G. Snellen^{1,2}, R.T. Schilizzi^{2,3}, G.K. Miley², A.G. de Bruyn^{4,5},
M.N. Bremer^{2,6,7}, H.J.A. Röttgering²

¹*Institute of Astronomy, Madingley Road, Cambridge CB3 0HA, United Kingdom*

²*Leiden Observatory, P.O. Box 9513, 2300 RA, Leiden, The Netherlands*

³*Joint Institute for VLBI in Europe, Postbus 2, 7990 AA, Dwingeloo, The Netherlands*

⁴*Netherlands Foundation for Research in Astronomy, Postbus 2, 7990 AA, Dwingeloo, The Netherlands*

⁵*Kapteyn Institute, Postbus 800, 9700 AV, Groningen, The Netherlands*

⁶*Institut d'Astrophysique de Paris, 98bis Boulevard Arago, 75014 Paris, France*

⁷*Department of Physics, Bristol University, H H Wills Physics Laboratory, Tyndall Avenue, Bristol, BS8 1TL, United Kingdom*

ABSTRACT

This paper describes an investigation of the early evolution of extra-galactic radio sources using samples of faint and bright Gigahertz Peaked Spectrum (GPS) and Compact Steep Spectrum (CSS) radio galaxies. Correlations found between their peak frequency, peak flux density and angular size provide strong evidence that synchrotron self absorption is the cause of the spectral turnovers, and indicate that young radio sources evolve in a self-similar way. In addition, the data seem to suggest that the sources are in equipartition while they evolve. If GPS sources evolve to large size radio sources, their redshift dependent birth-functions should be the same. Therefore, since the lifetimes of radio sources are thought to be short compared to the Hubble time, the observed difference in redshift distribution between GPS and large size sources must be due to a difference in slope of their luminosity functions. We argue that this slope is strongly affected by the luminosity evolution of the individual sources. A scenario for the luminosity evolution is proposed in which GPS sources increase in luminosity and large scale radio sources decrease in luminosity with time. This evolution scenario is expected for a ram-pressure confined radio source in a surrounding medium with a King profile density. In the inner parts of the King profile, the density of the medium is constant and the radio source builds up its luminosity, but after it grows large enough the density of the surrounding medium declines and the luminosity of the radio source decreases. A comparison of the local luminosity function (LLF) of GPS galaxies with that of extended sources is a good test for this evolution scenario. Unfortunately, only a handful of GPS sources are known at low redshift, and an LLF can only be derived, assuming that their cosmological number density evolution is similar to that of steep spectrum sources. The LLF derived in this way is shown to be in good agreement with the proposed evolution scenario. However, the uncertainties are large, and larger, homogeneously selected samples of GPS sources are needed.

1 INTRODUCTION

1.1 Gigahertz Peaked Spectrum and Compact Symmetric Objects.

An important element in the investigation of the evolution of extra-galactic radio sources is the study of young counterparts of ‘old’ FRI/FRII extended objects. Two classes of compact radio source can be found in the literature as most likely representatives of this early evolutionary stage: I) Gigahertz Peaked Spectrum (GPS) sources, which are characterised by a convex-shaped radio spectrum peaking at about 1 GHz in frequency (O’Dea 1998), and II) Compact Symmetric Objects (CSO) which are characterised by their small size (< 500 pc) and two-sided radio structure, e.g. having jets and lobes on both sides of a central core (Wilkinson et al. 1994). Clearly, samples of GPS sources

and CSOs are selected in very different ways. GPS sources are selected on their broadband radio spectra, while CSOs are selected on their multi-frequency milli-arcsecond morphology. Therefore studies of these objects have mostly been presented separately. However, a significant overlap between the two classes of sources exists. GPS sources optically identified with galaxies are most likely to possess compact symmetric radio morphologies (Stanghellini et al. 1997a, 1999), and the large majority of CSOs exhibit a gigahertz-peaked spectrum. The large but not complete overlap between these two classes of source is most likely caused by the synchrotron self-absorbed mini-lobes, located at the extremities of most CSOs, being the main contributors to the overall radio spectrum, and producing the peak at about 1 GHz in frequency.

1.2 Evidence for the young nature of GPS sources and CSOs.

Since the early discovery of GPS sources, it has been speculated that these were young objects (Shklovsky 1965, Blake 1970). However, a commonly discussed alternative to them being young was that they are small due to confinement by a particularly dense and clumpy interstellar medium that impedes the outward propagation of the jets (van Breugel, Miley & Heckman 1984; O’Dea, Baum & Stanghellini 1991). This latter hypothesis now looks less likely since recent observations show that the surrounding media of peaked spectrum sources are not significantly different from large scale radio sources, and insufficiently dense to confine these sources. The most compelling evidence for youth is found in observations of the propagation velocities of the hot spots of several GPS/CSOs (Owsianik & Conway 1998; Owsianik, Conway & Polatidis 1998; Tschager et al. 1999). They all appear to have separation velocities of typically $\sim 0.2h^{-1}c$, indicating a dynamical age of $\sim 10^3$ year and clearly showing that these are indeed young objects. Recent measurements of the high frequency breaks in Compact Steep Spectrum (CSS) sources, indicate that these somewhat larger objects have radiative ages in the range of 10^3 to 10^5 years (Murgia et al. 1999).

1.3 Current views on Radio Source Evolution

Observational constraints on the luminosity evolution of radio sources mainly come from the source density in the power - linear size ($P-D$) diagram (Shklovsky 1963). It was found that sources with large sizes ($D > 1$ Mpc, eg. Schoenmakers 1999) and high radio luminosities ($P > 10^{26}$ W/Hz at 178 MHz) are rare, suggesting that the luminosities of sources should decrease quickly with linear sizes approaching 1 Mpc. Several authors have compared the number densities of GPS and CSS sources with those of large radio sources to investigate the luminosity evolution of young radio sources (Fanti et al. 1995; Readhead et al. 1996; O’Dea & Baum 1997). Fanti et al. (1995) argue that the luminosities of CSS sources decrease by a factor of ~ 10 as they evolve to extended objects. Readhead et al. (1996) find a factor of 8 decrease in luminosity as a source expands from 500 pc to 200 kpc in overall size. Taking into account their CSO statistics, they find that the luminosity evolution in the phases CSO-MSO-LSO (MSO = Medium Symmetric Object; LSO = Large Symmetric Object), i.e. from 10 pc to 150 kpc, is consistent with a single power-law luminosity evolution. This conclusion is not supported by O’Dea & Baum (1997), who found that GPS and CSS sources must decrease in luminosity at a faster rate than the classical 3CR doubles. Blundell, Rawlings & Willott (1999) showed that any radio source evolution involving a decrease in luminosity with time would, at the highest redshifts, result in a bias towards young sources in flux density limited samples. Since this effect is only important at $z > 2-3$, it is not relevant to the analysis presented in this paper.

Several GPS and CSOs (eg. 0108+388; Baum et al. 1990) exhibit low level, steep spectrum, extended emission on arcsecond scales, which seem to be relics of much older radio-activity. These objects are often classified as being intermittent or re-occurrent, and therefore not as young ob-

jects. However, the components related to their gigahertz-peaked spectra and CSO morphologies are certainly young. The presence of faint relic emission only indicates that the active nucleus has been active before, and may constrain the typical timescale and frequency of such events. Based on the current knowledge of the formation of massive black-holes in the centers of galaxies, it is unlikely that the central engine itself is young, but just the radio source (Richstone et al. 1998).

It is unclear whether all young sources actually evolve to large extended objects. Some, or even the majority, may be short-lived phenomena due to a lack of significant fuel (Readhead 1994). The possible existence of these objects can have a large influence on the source statistics of young radio sources.

2 SAMPLES OF GPS AND CSS SOURCES

In this paper, we present a study of the evolution of young radio sources from the analysis of three samples of faint and bright GPS and CSS radio sources: The faint GPS sample from WENSS (Snellen et al. 1998a), the bright (Stanghellini et al. 1998) GPS sample, and the Fanti et al. (1990) CSS sample. As discussed in the companion paper (Snellen, Schilizzi & van Langevelde, 2000), we do not regard GPS quasars to be related to their galaxy counterparts; in the following we choose not to use the quasars for further analysis and only concentrate on the GPS and CSS galaxies. Unless stated otherwise, we will assume that *all* GPS galaxies evolve to large scale radio galaxies, and that *all* large scale radio galaxies were once GPS galaxies.

2.1 The faint GPS sample from WENSS

The selection of this sample has been described in detail in Snellen et al. (1998a). Candidate GPS sources were selected in two ways; i) with inverted spectra between 325 MHz and 625 MHz in WENSS (Rengelink et al. 1997), and ii) with inverted spectra between WENSS 625 MHz and Greenbank 5 GHz (Gregory & Condon 1991). The sources are located in two regions of the survey; one at $15^h < \alpha < 20^h$ and $58^\circ < \delta < 75^\circ$, which is called the *mini-survey* region (Rengelink et al. 1997), and the other at $4^h00^m < \alpha < 8^h30^m$ and $58^\circ < \delta < 75^\circ$. Additional observations at 1.4, 5, 8.4 and 15 GHz were carried out with the WSRT and the VLA, yielding a sample of 47 genuine GPS sources with peak frequencies ranging from 500 MHz to more than 15 GHz, and peak flux densities ranging from ~ 30 to ~ 900 mJy. This sample has been imaged in the optical and near-infrared, resulting in an identification fraction of $\sim 87\%$ (Snellen et al. 1998b, 1999). All the galaxies in the sample were used for the morphological evolution study. The redshifts of the majority of the objects had to be estimated from their optical magnitudes, using the well determined Hubble diagram for GPS galaxies (Snellen et al. 1996, O’Dea et al. 1996). Some, assumed to be galaxies, have only faint lower limits to their magnitudes. For these a redshift of $z=1.5$ was assumed.

The overall angular sizes were measured from the VLBI observations as the maximum angular separation of components or the angular size for single component source

Name	C	z	ν_{peak} (GHz)	S_{peak} (mJy)	P_{5GHz} (Log $\frac{W}{Hz}$)	θ (mas)
B0400+6042	+	1.5 ²	1.0	184	26.8	4.4
B0436+6152	+	1.5 ²	1.0	237	26.9	17.1
B0535+6743	+	1.5 ¹	5.7	192	27.2	4.0
B0539+6200	+	1.4 ¹	1.9	129	26.6	6.1
B0552+6017	-	1.5 ²	1.0	50	26.2	12.6
B0557+5717	-	1.2 ¹	1.1	69	26.2	6.5
B0752+6355	-	0.9 ¹	6.4	314	26.7	4.6
B0759+6557	-	1.5 ¹	1.7	46	26.2	8.0
B0830+5813	+	0.093	1.6	65	24.1	< 4.3
B1525+6801	+	1.1 ¹	1.8	163	26.5	22.4
B1551+6822	+	1.3 ¹	1.5	52	26.1	2.5
B1557+6220	+	0.9 ¹	2.3	49	25.8	< 4.4
B1600+7131	+	1.5 ²	1.7	346	27.0	22.7
B1620+6406	-	1.2 ¹	2.2	47	25.9	14.2
B1622+6630	+	0.201	4.0	363	25.5	< 2.9
B1639+6711	-	1.5 ²	1.0	68	26.4	< 4.1
B1655+6446	+	1.5 ²	1.0	69	26.3	24.8
B1657+5826	-	1.1 ¹	0.5	64	26.0	27.8
B1807+5959	-	1.0 ¹	1.0	47	25.9	13.0
B1807+6742	-	1.5 ²	0.8	54	26.2	6.9
B1808+6813	-	1.1 ¹	1.3	42	25.9	3.5
B1819+6707	-	0.220	0.8	338	25.5	19.2
B1841+6715	+	0.486	2.1	178	26.0	6.1
B1843+6305	-	1.5 ²	1.9	75	26.4	9.5
B1942+7214	+	1.1 ¹	1.4	233	26.7	31.5
B1946+7048	+	0.101	1.8	929	25.4	31.9

¹ estimate from optical magnitude

² assumed at z=1.5

Table 1. The GPS galaxies from the faint WENSS sample. The second column (+/-) indicates whether a source is part of the complete sub-sample or not.

(see companion paper) Their 5 GHz radio power was determined, assuming $H_0 = 50 \text{ km sec}^{-1} \text{ Mpc}^{-1}$ and $\Omega_o = 1$. For a few sources, the rest-frame peak frequency was above 5 GHz. The radio power of these galaxies was corrected for the spectral turnover by extrapolating their optically thin spectrum to rest-frame 5 GHz. In the most extreme case (B0752+6355), this correction is < 20%. B0531+6121 was omitted from the sample since it does not have a genuine GPS spectrum.

For the luminosity evolution study to be discussed in section 4, it is crucial to have a good understanding of the selection effects. We therefore applied more strict constraints than in the original sample. Only the GPS sources which have inverted spectra between 325 MHz and 5 GHz, and with flux densities of > 20 mJy at 325 MHz, 14 in total, were selected.

All the 26 galaxies in the sample are given in table 1. Column 1 gives the B1950 name, column 2 indicates whether the source is in the complete sub-sample or not, column 3 gives the (estimated) redshift, column 4 gives the observed peak frequency, column 5 the observed peak flux density, column 6 the rest-frame 5 GHz radio power, and column 7 the overall angular size.

2.2 The bright Stanghellini et al. GPS sample

A sample of radio bright GPS sources has been constructed by Stanghellini et al. (1998) from GPS candidates selected

Table 2. The complete sample of Bright GPS galaxies from Stanghellini et al. (1998)

Name	z	ν_{peak} (GHz)	S_{peak} (Jy)	P_{5GHz} (Log $\frac{W}{Hz}$)	θ (mas)	Refs.
0019-000	0.305	0.8	3.5	26.7	70	5
0108+388	0.669	3.9	1.3	27.3	6	6
0316+161	1.2	0.8	9.6	28.2	300	3
0428+205	0.219	1.0	4.0	26.6	250	3
0500+019	0.583	2.0	2.5	27.3	15	1
0710+439	0.518	1.9	2.1	27.1	25	7
0941-080	0.228	0.5	3.4	26.4	48	8
1031+567	0.459	1.3	1.9	26.9	33	9
1117+146	0.362	0.5	3.9	26.8	90	10
1323+321	0.369	0.5	7.0	27.1	60	3
1345+125	0.122	0.6	8.9	26.3	85	1
1358+624	0.431	0.5	6.6	27.1	80	3
1404+286	0.077	4.9	2.8	25.8	8	4
1600+335	1.1	2.6	3.1	27.9	60	3
1607+268	0.473	1.0	5.4	27.2	49	8
2008+068	0.7	1.3	2.6	27.3	30	2
2128+048	0.990	0.8	4.9	27.8	35	1
2210+016	1.0	0.4	4.5	27.7	80	1
2352+495	0.237	0.7	2.9	26.5	70	7

Refs for angular sizes:

- 1) Stanghellini et al. (1997a)
- 2) Stanghellini et al. (1999)
- 3) Dallacasa et al. (1995)
- 4) Stanghellini et al. (1997b)
- 5) Hodges, Mutel & Phillips (1984)
- 6) Owsianik et al. (1998)
- 7) Wilkinson et al. (1994)
- 8) Dallacasa et al. (1998)
- 9) Taylor, Readhead & Pearson (1996)
- 10) Bondi et al. (1998).

from the Kühr et al. (1981) 1 Jy catalogue, with declination > -25° and galactic latitude $|b| > 10^\circ$. Stanghellini et al. supplemented this data set with multi-frequency observations from the VLA, WSRT and data from the literature, and selected sources with a turnover frequency between 0.4 and 6 GHz, and an optical thin spectral index $\alpha_{thin} < -0.5$ at high frequency. The final complete sample consists of 33 GPS sources, of which 19 are optically identified with galaxies. Four galaxies do not have a spectroscopic redshift. Their redshifts were estimated from their optical magnitudes, in the same way as for galaxies in the WENSS-sample. Their rest-frame radio power at 5 GHz has also been calculated in the same way as for the objects in the WENSS sample.

All the galaxies in the sample are given in table 2. Column 1 gives the B1950 name, column 2 the redshift, column 3 the observed peak frequency, column 4 the observed peak flux density, column 5 the rest-frame 5 GHz radio power, and column 6 the overall angular size. Column 7 gives the reference for the angular size.

2.3 The Fanti et al. CSS sample

The sample of CSS sources used in this paper is from Fanti et al. (1990). They constructed a sample without spectral bias by integrating the 3CR sample with sources from the Peacock and Wall sample (1982) which would be stronger than 10 Jy at 178 MHz, if corrected for low frequency absorption by extrapolation of the straight high-frequency part of the spectrum. All sources were included with projected linear size < 15 kpc, (corrected) flux density at 178 MHz > 10 Jy, and with Log $P_{178} > 26.5$, in a well defined area

Table 3. The complete sample of CSS galaxies from Fanti et al. (1990).

Name	z	ν_{peak} (GHz)	S_{peak} (Jy)	P_{5GHz} ($\text{Log} \frac{W}{Hz}$)	θ ($''$)	Refs.
3C49	0.62	0.12	11	27.2	1.0	1
3C67	0.31	0.05	10	26.6	2.5	1
3C93.1	0.24	0.06	10	26.3	0.6	2
0404+76	0.59	0.60	6	27.6	0.1	2
3C237	0.88	0.05	40	27.9	1.2	1
3C241	1.62	0.04	17	27.8	0.8	1
3C268.3	0.37	0.08	11	26.9	1.3	1
3C299	0.37	0.08	13	26.8	11.5	1
3C303.1	0.27	0.10	10	26.4	2.0	1
3C305.1	1.13	0.09	10	27.5	2.8	1
3C318	0.75	< 0.04	20	27.3	0.8	1
3C343.1	0.75	0.25	13	27.6	0.3	1
3C346	0.16	< 0.04	10	26.2	2.3	1
1819+39	0.80	0.10	7	27.6	0.5	2
3C454.1	1.84	< 0.04	10	27.8	1.6	1

Refs for angular sizes:
 1) Spencer et al. 1989
 2) Dallacasa et al 1995

of sky ($|b| > 10^\circ$, $\delta > 10^\circ$). A number of sources, which are included in the Stanghellini et al. sample are omitted from the Fanti et al. sample to avoid duplication. The remaining CSS galaxies are listed in table 3.

3 THE SPECTRAL TURNS AND THE MORPHOLOGICAL EVOLUTION OF YOUNG RADIO SOURCES

Early measurements of the angular sizes of GPS and CSS sources using VLBI strongly suggested that their spectral turnovers are caused by synchrotron self absorption (SSA, Jones, O'Dell & Stein 1974; Hodges, Mutel & Phillips 1984; Mutel, Hodges & Phillips 1985) It was realised by Jones, O'Dell & Stein (1974) that if the optical depth due to SSA was less than unity at the spectral peak-frequency of these sources, lower magnetic fields, far from equipartition, would be present which should result in detectable self-compton radiation. Fanti et al. (1990) showed that there is a strong anti-correlation between the linear size and the turnover frequencies of CSS sources, as expected for SSA. However, more recently it was suggested by Bicknell, Dopita & O'Dea (1997) that such a correlation can also be explained by a particular model in which these sources undergo free-free absorption by ionised gas surrounding the lobes. In addition, Kuncic, Bicknell & Dopita (1998) argued that in addition to free-free absorption, induced Compton scattering will also have an important effect in forming the spectral peak. As a result, it opened up the debate again about the cause of the spectral turnovers in CSS and GPS sources.

The combination of bright and faint GPS and CSS samples as presented here, gives us a unique opportunity to carefully investigate the correlation between size and spectral peak. Not surprisingly, we confirm the anti-correlation between peak frequency ν_p and maximum angular size θ_{max} (see figure 1, top left panel). However, in addition we find a correlation between peak flux density S_p and θ_{max} . This is shown in the top right panel of figure 1. Note that only

sources from the bright and faint GPS samples are with $0.8 < \nu_p < 3$ GHz are plotted here. This is necessary, since the peak flux densities are correlated with the peak frequencies, which would erroneously result in a correlation between peak flux density and angular size.

From SSA theory, it is expected that the angular size θ of a radio source is proportional to (Kellerman & Pauliny-Toth, 1981):

$$\theta \propto B^{1/4} S_p^{1/2} (1+z)^{1/4} \nu_p^{-5/4} \quad (1)$$

where B is the magnetic field strength and z the redshift. Note that θ is only weakly dependent on both B and z . Most remarkably, the strength and signs of the correlations between ν_p , S_p and θ_{max} as shown in figure 1 are exactly as expected from equation 1.

The overall angular size, θ_{max} (eg. the distance between the two mini-lobes), is used in the analysis above, but θ in equation 1 corresponds to the size of the radio *components* which are dominant at the peak-frequency (the mini-lobes). Therefore, these correlations have implications for the morphological evolution of these radio sources. The lower left panel of figure 1 shows the maximum angular size as function of $S_p^{1/2} \nu_p^{-5/4}$. The solid line indicates the best linear fit. The dependence of this relation on redshift is proportional to $(1+z)^{1/4}$, which in any case is smaller than < 20% and negligible for our z-range. Therefore the same relation is expected in the rest-frame of the objects. In the rest-frame, we can solve for the magnetic field B by assuming equipartition. For this we use the equation derived by Scott & Readhead (1977) assuming an optically thin spectral index $\alpha = -1$,

$$L = 3.5 \times (1 - (1+z)^{-1/2})^{-1/17} (1+z)^{1/2} S_p^{8/17} \nu_p^{33/34} \quad (2)$$

where L is the equipartition component size. The projected linear size is shown as function of the equipartition component size in the lower right panel of figure 1. The dashed line indicates the dependence for which both quantities are the same. The solid line is the best linear least-squares fit, indicating a ratio of overall size to component size of 5–6, throughout the samples of faint and bright GPS and CSS galaxies. This means that if GPS sources evolve into CSS sources, their ratio of component size to overall linear size remains constant, implying a self-similar evolution.

Note that the main difference between the lower left and right panels of figure 1 is that in the first a constant magnetic field is assumed, and in the second an equipartition magnetic field. It appears that the first correlation is slightly flatter than expected for self-similar evolution. Indeed the ratio of the component to overall angular size is on average a factor 2 smaller for the CSS sample than for the GPS samples, while these ratios are virtually the same assuming an equipartition magnetic field. This may indicate that young radio sources stay in equipartition while evolving in a self-similar way. This would require that the magnetic fields in CSS sources are typically a factor ~ 20 lower than in GPS sources. The linear correlation itself only indicates a constant ratio between the magnetic field and particle energies. This constant does not have to be equal to unity, as required for equipartition. However, for a ratio of unity in energies, the bottom right panel of Figure 1 requires a ratio of overall to component size of typically 5–6, which is close to the result seen in VLBI observations. This means that

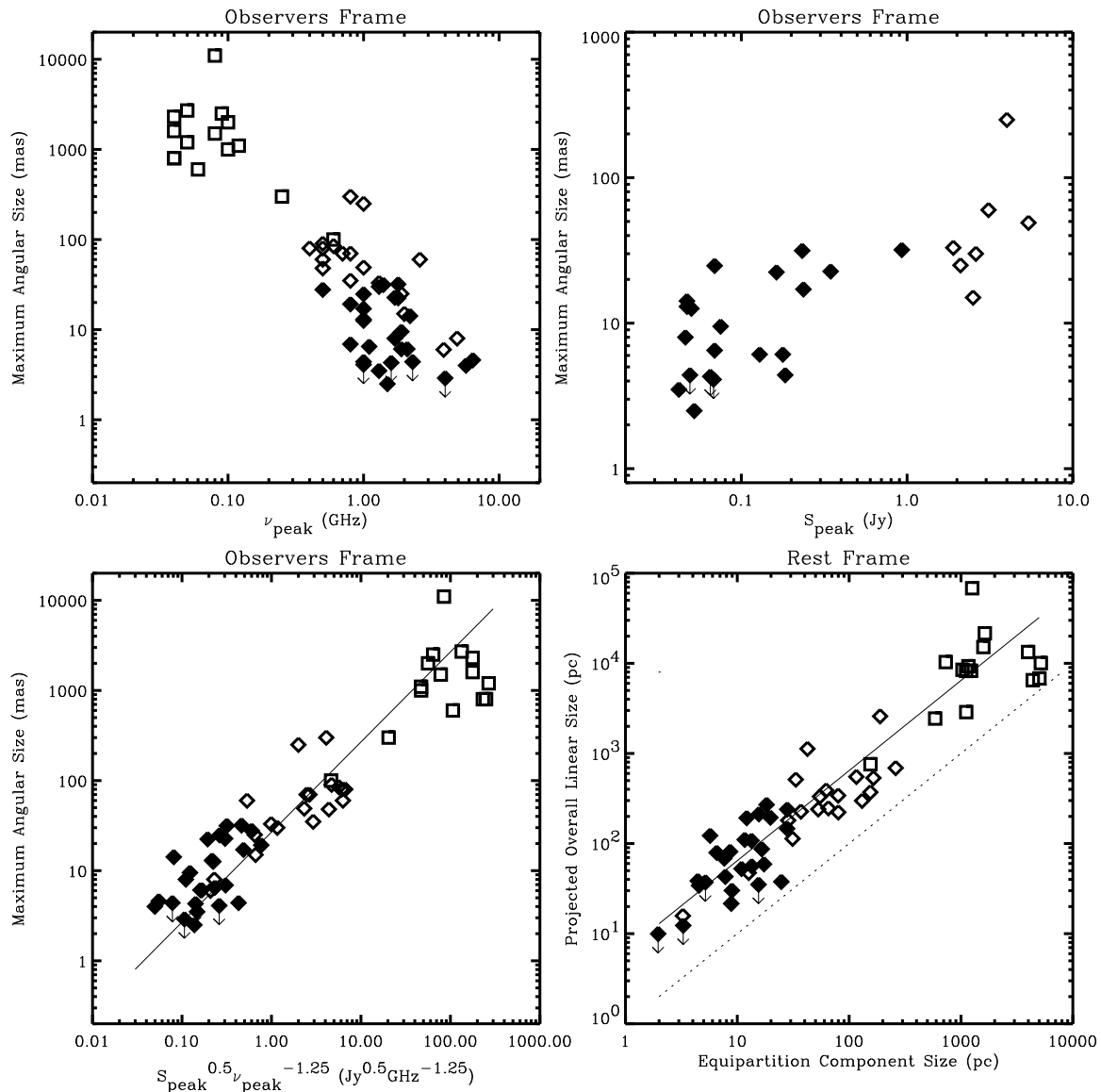


Figure 1. Correlations found between the spectral turnover and the overall size in samples of GPS and CSS sources. Squares, open and filled diamonds indicate objects from the CSS, bright and faint GPS sample respectively. (top left) The maximum angular size versus peak frequency. (top right) The maximum angular size versus peak flux density for sources with $0.8 < \nu_p < 3$. (bottom left) The maximum angular size versus $S_p^{1/2} \nu_p^{-5/4}$. The line indicates a linear correlation between the two parameters. (bottom right) The overall linear size versus the equipartition component size. The distance of the data-points to the dotted line indicates the component to overall size ratio.

the energy ratio is not only constant, but also close to unity, which indicates that equipartition probably holds.

Figure 1 demonstrates that the data is consistent with a combination of SSA, equipartition, and self-similar growth. It is not obvious that the same correlation should apply for free-free absorption. Although other more complicated combinations of mechanisms such as free-free absorption with induced Compton scattering (Kuncic, Bicknell & Dopita, 1998) may also fit the data, the simplest explanation by far is to assume that SSA, equipartition and self-similar source growth all individually hold. We therefore believe that SSA

is indeed the cause of the spectral turnovers in GPS and CSS sources.

It may not be surprising that young radio sources evolve in a self-similar way. Leahy and Williams (1984) showed that the cocoons of FR II sources of very different physical size had similar axial ratios. More recently, Subrahmanyan, Saripalli & Hunstead (1996) found very similar ratios for sources of linear sizes above 900 Kpc, also suggesting that radio sources evolve in a self-similar way. An analytical model for radio sources with pressure confined jets developed by Kaiser & Alexander (1997) shows that the properties of the bow shock and of the surrounding gas *force* the sources to

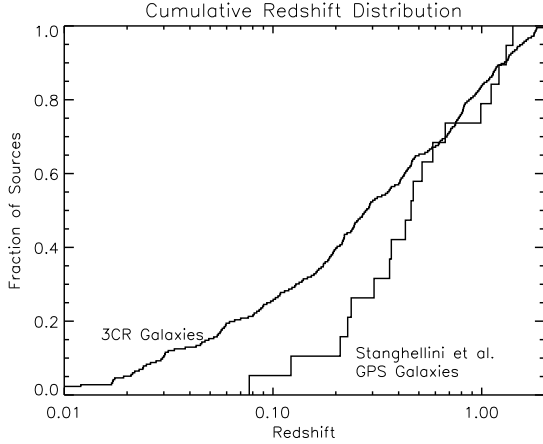


Figure 2. The cumulative redshift distribution for 3C galaxies and GPS galaxies from the Stanghellini et al. sample.

grow in a self-similar way, provided that the density of the surrounding gas falls off less steeply than $1/r^2$.

4 THE LUMINOSITY EVOLUTION OF YOUNG RADIO SOURCES

The number count statistics and linear size distributions used in studies to constrain the luminosity evolution of radio sources, have all been averaged over a wide redshift range and only include the brightest objects in the sky (Fanti et al. 1995, Readhead et al. 1996, O’Dea & Baum 1997). However, in flux density limited samples, the redshift distribution of GPS galaxies is significantly different from that of large size radio galaxies (see figure 2). This suggests that the interpretation of the number count statistics is not straightforward. Note that given the expected luminosity evolution as sources evolve in size, many of the present day GPS sources will have FRI luminosities. It is therefore assumed that GPS galaxies evolve into both FRI and FRII sources.

The bias of GPS galaxies towards higher redshifts than large size radio galaxies itself provides an important clue about the luminosity evolution of radio sources. It implies that GPS galaxies are more likely to have higher radio power than extended objects in flux density limited samples. If GPS and large size radio sources are identical objects, observed at different ages, their cosmological density evolution, for example their birth rate as function of redshift, should be the same. Since their lifetimes are short compared to the Hubble time, the redshift distributions of the GPS galaxies, and the objects they evolve to, should also be the same. The bias of GPS sources towards higher redshifts and radio powers therefore implies that their luminosity function must be flatter than that of large size radio sources. We argue that the luminosity evolution of the individual objects strongly influences their collective luminosity function, and propose an evolution scenario in which GPS sources increase in luminosity and large size sources decrease in luminosity with time (see section 4.1). In the simplified case, in which source to source variations in the surrounding medium can be ignored, the luminosity of a radio source depends only on its age and jet power. Consider first the luminosity function

of large size sources. It is expected that large size sources decrease in luminosity with age (see section 4.1). Therefore high luminosity sources will tend to be biased towards objects with both small ages and high jet powers. The intrinsic space density for high power jet sources will of course tend to be small. Furthermore, for a given jet power there are fewer young sources than old sources, simply because sources spend only a small fraction of their time being young. The result is a very low space density of large size sources of high power. In contrast, large size sources of low power are biased to be both old and with low jet power, both common conditions, hence the space density of large size sources with low power is much higher than that for those with high power, and the luminosity function for large size sources is steep. In contrast, the luminosity of GPS sources is expected to increase with sources age (see section 4.1). High luminosity GPS sources are therefore biased to be old and of high jet power, while low luminosity objects are biased to be young and of low jet power. Instead of reinforcing each other as in the case for large size sources, for GPS sources the age and jet power space density biases partly counteract. The result is a much less difference in the space density of low and high power GPS sources and hence a much flatter luminosity function for GPS sources.

In the next section we will show that the luminosity evolution as proposed is expected for a ram-pressure confined, self similarly evolving radio source in a surrounding medium with a King-profile density. In the inner parts of the King profile, the density of the medium is constant and the radio source builds up its luminosity (eg. Baldwin 1982), but after it grows large enough the density of the medium declines and the luminosity of the radio source decreases.

In section 4.2 we will show how the luminosity evolution of the individual sources modifies the luminosity function, and in section 4.3, the local luminosity function of GPS sources is constructed and compared with that of large size radio sources.

4.1 A self-similar evolution model

An important parameter in evolution models of radio sources is the density profile of the surrounding medium. In general, X-ray observations of nearby ellipticals have shown that their ISM are well fitted by a King profile distribution (Trinchieri et al. 1986):

$$\rho(r) = \rho_0 \left[1 + \left(\frac{r}{r_c} \right)^2 \right]^{-\beta/2} \quad (3)$$

where ρ is the density of the medium as function of distance to the centre of the host galaxy r , r_c is the core radius, and β the slope parameter. Typical core radii in giant ellipticals are observed to be $r_c = 500 - 1000$ pc (Trinchieri et al. 1986), For simplicity, we treat the two regimes separately: 1) The GPS phase at $r < r_c$ where the density of the medium, ρ_{ism} , is assumed to be constant. 2) The large size (LS) phase at $r > r_c$ where $\rho_{ism} \propto r^{-\beta}$.

If the thrust of the radio jet is balanced by the ram-pressure of the surrounding medium, the growth of the radio source is equal to

$$dr/dt \propto \left(\frac{P_J}{\rho_{ism}(r)A} \right)^{1/2} \quad (4)$$

where dr/dt is the propagation velocity of the hot-spots, P_J is the jet power, and A is the cross-sectional area (Begelman 1996). In the previous section we showed that young radio sources seem to evolve in a self-similar way. Since it is in close agreement with the theoretical work of Kaiser & Alexander (1997), we will assume self-similar evolution, with $A \propto r^2$. Note however, that in the work by Kaiser & Alexander (1997), the cross-sectional area of the jet grows slightly more slowly with size, which is therefore not completely self-similar, but allowing the expansion of the bow-shock and cocoon to be fully self-similar (Kaiser 2000, private communications). Here, by assuming $A \propto r^2$, this will not be the case, but differences are small and for simplicity's sake we use this anyway.

From integrating eq. 4 it follows that in the GPS phase a source grows in linear size with time as $t^{1/2}$, assuming that the jet-power is constant with time. The average internal density of the radio source, ρ_i , is proportional to $P_J t/V$, where V is the volume of the radio source which is proportional to r^3 . Hence, $\rho_i \propto r^{-1}$, indicating that the radio emitting plasma expands proportionally to its linear size, r , and that expansion losses have to be taken into account. If the energy spectrum of the electrons is $n(E) = n_o E^{-\gamma}$, n_o varies proportionally to $r^{-4/3}$ for $\gamma = 2$ ($\alpha = -0.5$, Moffet, 1977). We will assume that the radio source is in equipartition, so that $n_o \propto B^2$, where B is the magnetic field. The radio power L_ν at a particular frequency in the optically thin part of the spectrum scales as

$$L_\nu \propto n_o^{7/4} V \propto P_J^{7/8} r^{2/3} \quad (5)$$

for $\gamma = 2$. Hence radio sources increase in luminosity in the GPS phase.

In the LS phase, radio sources grow as $t^{2/(4-\beta)}$, and the density of the radio emitting plasma varies as $\rho_i \propto r^{-\frac{\beta+2}{2}}$. Taking into account expansion losses in a similar way as for the GPS phase, this means that $n_o \propto r^{-4\frac{\beta+2}{6}}$, and under equipartition conditions,

$$L_\nu \propto P_J^{7/8} r^{\frac{2}{3} - \frac{7}{6}\beta} \quad (6)$$

Hence radio sources in the LS phase decrease in radio luminosity. Note that we do not take synchrotron losses and losses due to scattering of the CMB into account, which may influence the LS phase and cause sources to decrease faster in luminosity with time. The schematic evolution in radio power of a radio source according to this model is shown in figure 3.

It is interesting to determine what the expected evolution in peak frequency and peak flux density is for a radio source in the GPS phase and the LS phase. A source will become optically thick at a frequency where $\kappa_\nu l \approx 1$, where κ_ν is the absorption coefficient and l the pathlength through the radio plasma. For synchrotron self absorption, assuming equipartition and self-similar evolution, this means that,

$$\kappa_\nu l \propto n_o B^2 \nu_p^{-3} r \propto n_o^2 \nu_p^{-3} r = 1 \quad (7)$$

for $\gamma = 2$ (Moffet, 1977). The optically thin radio power, as determined above, will be frequency dependent and proportional to $P_\nu \propto S_p \nu_p^{1/2}$. Therefore in the GPS phase,

$$\nu_p \propto r^{-5/9}, \quad S_p \propto r^{17/18}, \quad S_p \propto \nu_p^{-17/10} \quad (8)$$

In the LS phase, assuming $\beta = 1.5$, which is a typical value

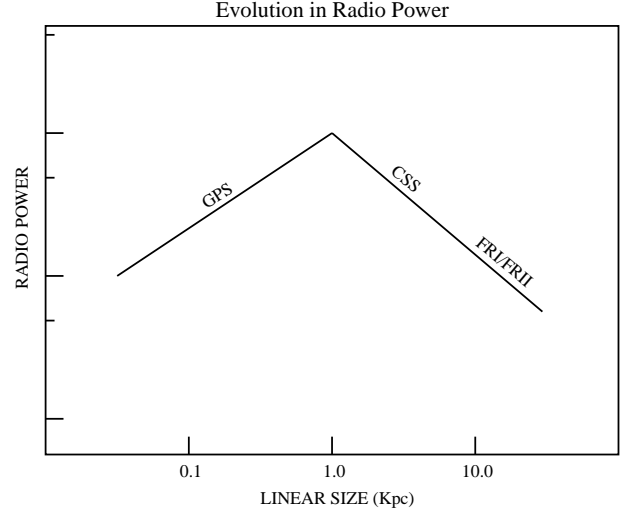


Figure 3. The evolution in radio power as function of linear size for a self-similar evolving, ram-pressure confined radio source in a surrounding medium with a King-profile density.

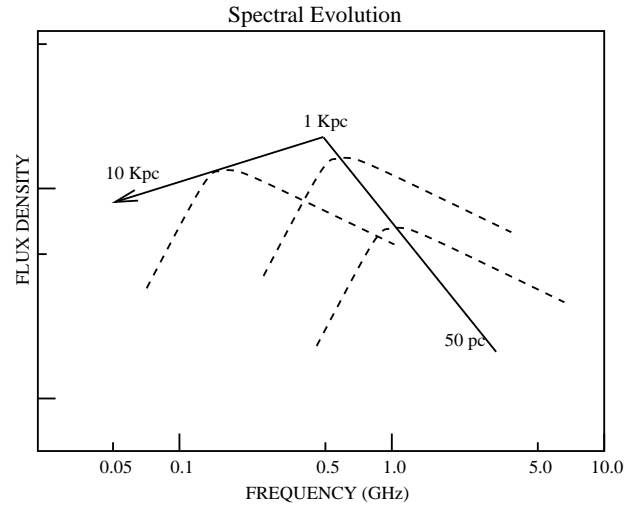


Figure 4. An evolutionary track for a self-similar evolving, ram-pressure confined radio source in a surrounding medium with a King-profile density

based on observations of X-ray halos (Trinchieri et al. 1986),

$$\nu_p \propto r^{-11/9}, \quad S_p \propto \nu_p^{17/44} \quad (9)$$

From figure 1 we can estimate the transition between the two phases (500-1000 pc) to occur at $\nu_p \approx 100 - 500$ MHz. The evolutionary tracks are shown in figure 4.

4.2 Luminosity evolution and the luminosity function.

In this section the influence of the luminosity evolution of the individual objects on the slope of their collective luminosity function is derived. We will ignore source to source variations in the surrounding medium and use the radio-size dependent luminosity evolution as derived in the previous section.

Suppose that the comoving number density of sources

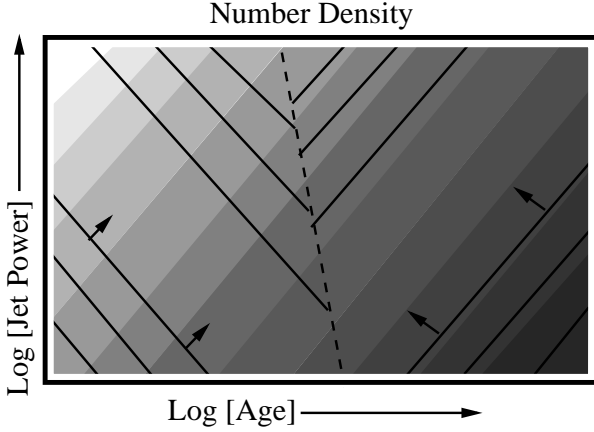


Figure 5. Schematic representation of the source density as function of age and jet power. The lines indicate sources with identical luminosities. The greyscales indicate the source density for a particular jet power and age. The dashed line indicates the border between the GPS phase and the LS phase.

with a jet power $N(P_J)$ is a power-law distribution

$$N(P_J) \propto P_J^\delta \quad (10)$$

between P_- and P_+ , and the sources have a flat distribution of ages below a certain maximum age, then the source density as function of age and jet power is represented by the grey scales in figure 5. The radio power of a source, L_ν , can be parameterised as

$$L_\nu \propto P_J^\kappa r^\epsilon \quad (11)$$

where $\epsilon = 2/3$ and $\epsilon = -13/12$ in the GPS phase and LS phase respectively, and $\kappa = 7/8$, as derived in the previous section. A line-integral over a solid line in figure 5 gives the total number of sources in the volume with a particular luminosity. It can be seen that in the GPS phase, these lines are approximately perpendicular to the density gradient, indicating that a change in luminosity results in only a small change in the number of sources. In the LS phase, they are parallel to the density gradient, and a change in luminosity results in a large change in the number of objects. The luminosity function $N(L)$ can be derived from,

$$N(L_\nu) = \frac{\delta}{\delta L_*} \iint_{L_\nu(p,r) < L_*} N(p,r) dp dr \quad (12)$$

where p is the jet power and r is the size of the radio source. As can be seen in figure 5, the integration limits of this equation are a different function of age and jet power, depending on the luminosity. The equation should be solved separately for a high and low luminosity regime, in both the LS and the GPS phase. Since the border between the GPS and LS phase is at a constant source size, r_* , it is better to integrate over the source size r than over the source age t . For the low luminosity regime in the GPS phase,

$$N(L_\nu < L_*) = \int_{P_-}^{P_+} \int_0^{\frac{L_*^{1/\epsilon}}{p^{\kappa/\epsilon}}} p^{\delta - \frac{1}{2}} r dr dp = L_*^{\frac{2}{\epsilon}} \int_{P_-}^{P_+} p^{\delta - \frac{1}{2} - \frac{2\kappa}{\epsilon}} dp \quad (13)$$

where $N(L_\nu < L_*)$ are the total number of sources below a particular luminosity L_* , and therefore integrating over jet power p and age t gives,

$$N(L_\nu) \propto L_\nu^{2/\epsilon - 1} \quad (14)$$

For the high radio power regime in the GPS phase,

$$N(L_\nu > L_*) = \int_{\left(\frac{L_*}{P_+^\kappa}\right)^{\frac{1}{\epsilon}}}^{r_*} r \int_{\left(\frac{L_*}{r^\epsilon}\right)^{\frac{1}{\kappa}}}^{P_+} p^{\delta - \frac{1}{2}} dp dr \propto L_*^{(\delta + \frac{1}{2})\frac{1}{\kappa}} \quad (15)$$

with a sharp cut-off near $L_\nu = P_+^\kappa r_*^\epsilon$. In this regime of radio power,

$$N(L_\nu) \propto L_\nu^{(\delta + \frac{1}{2})\frac{1}{\kappa} - 1} \quad (16)$$

For the low luminosity regime in the LS phase,

$$N(L_\nu < L_*) = \int_{p_-}^{\left(\frac{L_*}{r_+^\epsilon}\right)^{\frac{1}{\kappa}}} p^{\delta - \frac{1}{2}} \int_{\left(\frac{L_*}{p^\kappa}\right)^{\frac{1}{\epsilon}}}^{r_+} r^{\frac{1}{2}} dr dp \propto L_*^{(\delta + \frac{1}{2})\frac{1}{\kappa}} \quad (17)$$

with a sharp cut-off near $L_\nu = P_+^\kappa r_+^\epsilon$. In this regime of radio power,

$$N(L_\nu) \propto L_\nu^{(\delta + \frac{1}{2})\frac{1}{\kappa} - 1} \quad (18)$$

For the high radio power regime in the LS phase,

$$N(L_\nu > L_*) = \int_{r_*}^{\left(\frac{L_*}{P_+^\kappa}\right)^{\frac{1}{\epsilon}}} r^{\frac{1}{2}} \int_{\left(\frac{L_*}{r^\epsilon}\right)^{\frac{1}{\kappa}}}^{P_+} p^{\delta - \frac{1}{2}} dp dr \propto L_*^{3/2\epsilon} \quad (19)$$

with a cut-off near $L_\nu = P_+^\kappa r_*^\epsilon$. In this radio power regime,

$$N(L_\nu) \propto L_\nu^{3/2\epsilon - 1} \quad (20)$$

As can be seen from equations 15 and 18, the slope of the luminosity function is expected to be the same in the high luminosity and low luminosity regimes for the GPS and LS phases respectively, since δ and κ are independent of the age of the radio source. The low luminosity regime and the high luminosity regime of the GPS phase and the LS phase are expected to have a slope of +2 and -2.4 respectively for the proposed evolution model.

4.3 The Local Luminosity Function of GPS sources.

As is shown in the previous section, the comparison of the local luminosity function (LLF) of young and old radio sources can put strong constraints on the rise and decay of their radio luminosity. One would like to compare the LLF of GPS sources with the model derived in section 4.1 & 4.2 directly. This is not possible due to the lack of local GPS sources in present samples (the low local number density of GPS sources catalysed this discussion in the first place). For example, only 2 GPS galaxies in the Stanghellini et al. sample are at $z < 0.2$. However, since we assume that GPS sources evolve into large size sources and their lifetimes are

short compared to cosmological timescales, their birth rate as function of redshift should be the same. Therefore the cosmological evolution as determined for large scale radio sources can be used to describe the cosmological evolution for GPS sources. In this way, the GPS LLF can be estimated using the GPS galaxies at all redshifts, which will be attempted in this section. This estimated GPS LLF will then be compared with what is expected from the model, as derived in section 4.2.

The LLF for powerful radio sources and its cosmological evolution, has been studied by Dunlop & Peacock (1990). We will use the pure luminosity evolution model, since it fits the available redshift and source-count data well, and it is relatively straightforward to implement. In this particular model, the overall shape of the luminosity function does not change with cosmological epoch, only the normalisation in luminosity (see fig. 6). Dunlop and Peacock (1990) parameterise an evolving two-power-law luminosity function as

$$\rho(P_\nu, z) = \rho_o \left\{ \left(\frac{P}{P_c(z)} \right)^a + \left(\frac{P}{P_c(z)} \right)^b \right\}^{-1} \quad (21)$$

where a and b are the two power-law slopes, $P_c(z)$ is the evolving ‘break’ luminosity, and ρ_o is determined by normalisation at $z=0$. The redshift dependence, $P_c(z)$, was parameterised by Dunlop & Peacock as

$$\log P_c(z) = a_0 + a_1 z + a_2 z^2 \quad (22)$$

The best-fit model parameters for pure luminosity evolution ($\Omega_0 = 1$) are, $\rho_o = -6.91$, $a = 0.69$, $b = 2.17$, $a_0 = 25.99$ (in W/Hz), $a_1 = 1.26$, $a_2 = -0.26$. Since Dunlop & Peacock (1990) did their analysis at 2.7 GHz, their radio powers have to be transformed to 5 GHz. Assuming a mean spectral index of -0.75 , we use a conversion factor of -0.20 in the logarithm. This luminosity evolution parameterisation, as shown in figure 6, is used to derive the LLF of GPS sources. First the radio powers, as given in table 1 and 2, are corrected for the cosmological evolution of the luminosity function. This correction factor as function of redshift is equation 22. For example, at $z=1$, the luminosity function has shifted a factor 10 towards higher luminosities, and therefore 2128+048 with a radio power of $10^{27.8}$ W/Hz will contribute to the LLF at $10^{26.8}$ W/Hz. Note that this correction is independent of luminosity, and therefore the difference in radio luminosity of young and old sources does not have to be accounted for. Note however, that the increase in number density *is* dependent on radio luminosity due to a change in the slope of the luminosity function. The number densities increase from $z=0$ to $z=1$ by a factor of 5 and 150 for low and high luminosity sources respectively.

Figure 7 shows the corrected and uncorrected radio powers for a source with flux densities of 10 mJy, 100 mJy and 1 Jy (assuming a spectral index of -0.5 at about 5 GHz). Interestingly, the corrected radio power for a source with an certain observed flux density, does not significantly change at $0.6 < z < 2.0$. Hence, although for many GPS galaxies no spectroscopic redshift has been measured, this is not likely to influence the result, since they will probably all be in this redshift range.

The next step is to correct the number of sources observed for the volume of space over which they can be observed. As can be seen from figure 7, a flux density limit

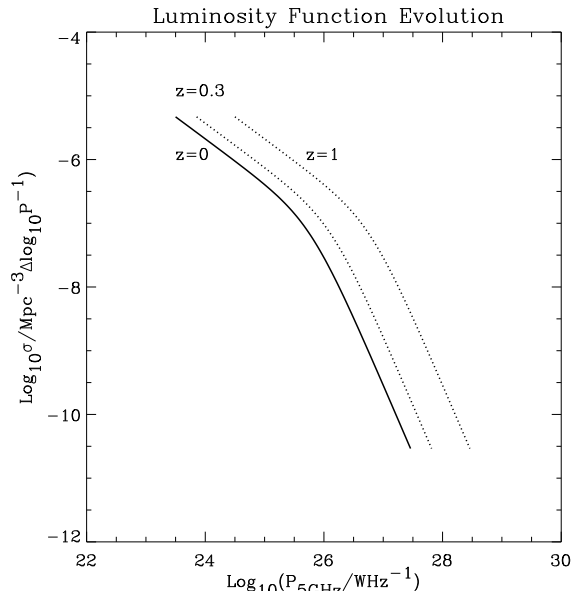


Figure 6. The evolution of the luminosity function of steep spectrum sources as determined by Dunlop and Peacock (1990).

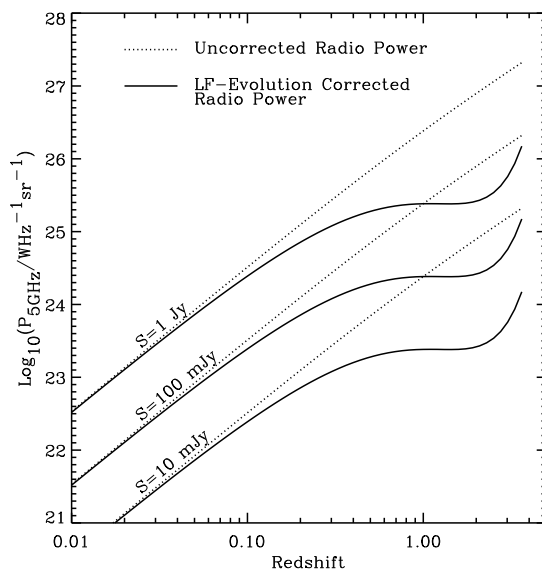


Figure 7. The radio power for a source of 10 mJy, 100 mJy, and 1 Jy as function of redshift, and its radio power corrected for the evolution of the luminosity function, assuming $H_0=50$ km $\text{sec}^{-1}\text{Mpc}^{-1}$, and $\Omega_0=1$.

in the sample of 1 Jy means that all sources with corrected luminosities greater than $25.4 \text{ W Hz}^{-1} \text{ Sr}^{-1}$ can be detected out to $z=2$, and that only source with lower radio power, and consequently at $z < 0.6$, have to be corrected for the fact that they only could have been seen out to a certain redshift. However, a possible additional redshift limit results from the lower limit in peak frequency at 0.4 GHz in the bright Stangellini et al. sample, and in the faint sample due to the limit in 325-5000 MHz spectral index. For these sources a weight-factor is used equal to the volume of the survey (assuming a

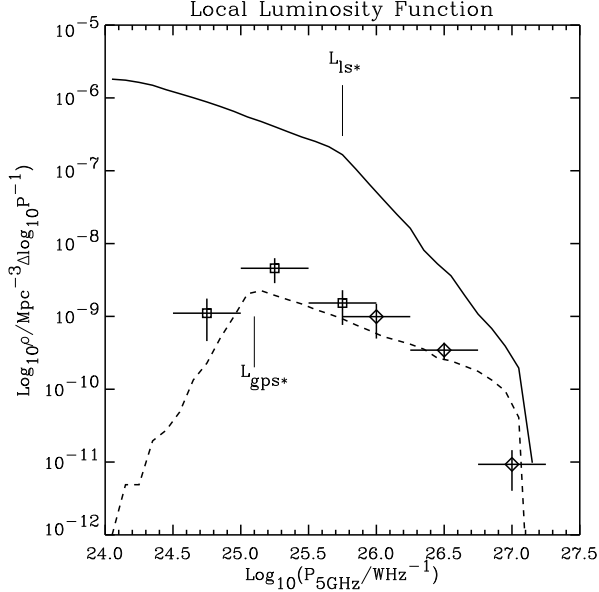


Figure 8. The local luminosity function of GPS radio sources, as derived from the bright sample of Stanghellini et al. (diamonds) and our faint GPS sample (squares). The dashed and solid lines give the simulated LLFs for GPS and large size radio sources respectively. The model-parameters are chosen in such way that the simulated LLF of large size radio sources matches that of steep spectrum sources as derived by Dunlop & Peacock (1990).

redshift limit of 2.0) divided by the maximum volume over which they could have been in the sample, which is dependent on the maximum observable redshift. The corrections above are relatively straight-forward. However, some additional, more complicated corrections have to be made for the faint GPS sample. Firstly, this sample is originally selected at 325 MHz frequency, eg. on the optically thick part of their spectrum. Furthermore, only sources with positive spectral indices between this frequency and 5 GHz were initially selected. Therefore the faint WENSS sample is more biased towards GPS sources with higher peak frequencies than the bright Stanghellini et al. sample. To correct for this we assumed that the parent distribution of peak frequencies is independent of flux density and radio power, and determined what fraction of the Stanghellini et al sample would have been included in the sample if it would have been selected as for the faint WENSS sample. It turns out that 26 % of the galaxies in the bright sample have 325 MHz flux densities > 1 Jy and positive spectral indices between 325 MHz and 5 GHz. In addition, the bright GPS sample has a limit in optically thin spectral index of -0.5 , while several sources in the faint sample have a flatter optically thin spectral index. Taking into account these two effects, the number densities for the faint sample are multiplied by a factor 3.2.

The resulting local luminosity function of GPS sources is shown in figure 8. Note that a luminosity bin (centred at 23.75 Watt/Hz) containing only a single source (B0830+5813) is omitted due to its large uncertainty.

We compared the resulting LLF with an LLF of a simulated radio source population of 10^6 objects, with random ages, and a jet-power distribution defined as in equation 10.

Table 4. Dependence of LLF characteristics on the model parameters

Characteristic of LLF	Dependence	Value used
LS-LLF slope at high L	$\frac{5+7\beta}{4-7\beta}$	-3.17^a
LS-LLF slope at low L	$(\delta + \frac{1}{2})\frac{1}{\kappa} - 1$	-1.69^a
L_{max}	P_+^κ	$10^{27.1}$
L_{ls*}	$P_+^\kappa \left(\frac{r_+}{r_*}\right)^{\frac{2}{3} - \frac{7}{6}\beta}$	$10^{25.8^a}$
L_{gps*}	P_-^κ	$10^{25.0}$

^a Value chosen to match the LLF of Dunlop & Peacock (1990).

The ‘observed’ luminosity of a source was calculated assuming that it had evolved over its lifetime according to the luminosity evolution derived in section 4.1, out to a maximum size, r_+ . At $r < r_*$, the size of the source evolves as $r = t^{1/2} P_J^{1/4}$. To avoid a discontinuity in propagation velocity at r_* , the source evolves from r_* as,

$$r(P_J, t) = \frac{\gamma}{2} \gamma^{-\frac{1}{\gamma}} (\gamma P_J^{\frac{1}{2}} t)^{\frac{1}{\gamma}} + (1 - \frac{\gamma}{2}) \quad (23)$$

with $\gamma = (4 - \beta)/2$. The luminosity of a source increases at $r < r_*$ as $L = P_J^{7/8} (r/r_*)^{2/3}$, and as $L = P_J^{7/8} (r/r_*)^{\frac{2}{3} - \frac{7}{6}\beta}$ at $r > r_*$. This results in a similar evolution for large size radio sources as derived in section 4.1, with the luminosity at $r = r_*$ only dependent on P_J . It was not our aim to determine absolute values for number densities and radio powers with these simulations. The results of the simulation were scaled in such way, that the LLF obtained for large size radio sources, matched the LLF of steep spectrum sources as derived by Dunlop & Peacock (1990).

Table 4 lists the important characteristics of the simulated LLF of large size and GPS sources, and their dependence on the free model parameters. The parameters δ and β , as defined in equations 10 and 3, determine the slope of the low and high luminosity part of the LLF of large size radio sources. These were chosen to be similar to the parameters $a - 1$ and $b - 1$ as derived by Dunlop & Peacock (1990), with $\delta = -1.10$ and $\beta = 1.16$. This value of β is slightly lower than derived from X-ray observations of nearby ellipticals ($\beta = 1.5 - 2$, Trinchieri et al. 1986). Note however, that the radio source population is dominated by objects with size > 20 kpc, for which the surrounding medium is dominated by intra-cluster gas, which is expected to have a flatter density gradient. With the parameters δ and β and the slopes of the LLF of large size radio sources fixed, the relative positions of the break luminosities could be determined. A sharp cut-off will occur near the highest luminosity, L_{max} . The number of GPS galaxies in the highest luminosity bin, as shown in figure 8, is lower than expected from the extrapolation of the LLF at lower luminosities. This can be explained if this luminosity bin is near the cut-off luminosity L_{max} . We therefore chose $\log L_{max}$ to be 27.1 (W Hz $^{-1}$). The break luminosity of large size radio sources, is also determined by Dunlop & Peacock (1990) to be $\log L_{LS*} = 25.79$ (corrected to 5 GHz). As can be seen from table 4, the luminosity ratio L_{max}/L_{ls*} determines the value of r_+/r_* . This corresponds to a maximum size for a radio source of

100 kpc, assuming $r_* = 1$ kpc. This value is quite near the turnover seen in the linear size distribution of 3CR galaxies, as shown by O’Dea & Baum (1997). The break luminosity of GPS sources, L_{gps*} , relative to L_{max} , is dependent on the range of jet-powers (P_+/P_-). To let L_{gps*} coincide with the peak in the observed GPS LLF, a value of $(P_+/P_-)=200$ was used.

Although the uncertainties on the datapoints are large and several free parameters enter the simulation, figure 8 shows that the shape of the LLF of GPS sources is as expected. Note that most free parameters are determined by fitting the LLF of large size radio sources to that of Dunlop & Peacock (1990), except r_+ and (P_+/P_-) . This analysis should be regarded as an example of how future large and homogeneously defined samples of GPS sources can constrain the luminosity evolution of extragalactic radio sources.

The proposed increase in luminosity for young radio sources seems to be in contradiction to the high number counts of GPS sources with respect to large size radio sources suggesting that they should decrease in radio luminosity by a factor 10 during their lifetime (Fanti et al. 1995, Readhead et al. 1996, O’Dea & Baum 1997). However, this is not the case. Flux density limited samples, as used for these analyses, only probe the most luminous objects at any redshift. As can be seen from figure 8, at high luminosities, the two luminosity function approach each other, due to the flatter slope of the luminosity function of GPS sources. This results in a relatively high number density of GPS sources in flux density limited samples.

4.4 Summary and Conclusions

In this paper we show that in addition to the well known correlation between spectral peak frequency and angular size (eg. Fanti et al. 1990), a correlation exists between the peak flux density and angular size of GPS & CSS sources. The strength and sign of these correlations are exactly as expected from SSA theory, assuming equipartition, and are therefore a strong indication that SSA is indeed the cause of the spectral turnovers in these objects. Furthermore, these correlations are consistent with GPS & CSS sources evolving in a self-similar way. Interestingly, the self-similar evolution scenario is better fitted by assuming an equipartition than a constant magnetic field.

In flux density limited samples, GPS galaxies are found at higher redshifts than large size radio sources. Since the lifetimes of radio sources are short compared to cosmological timescales, this can only mean that the slope of their luminosity functions are different, if GPS sources are to evolve into large size radio sources. It is shown that that the slope of a luminosity function is strongly dependent on the evolution of radio power of the individual sources. A new method is introduced to constrain the luminosity evolution of radio sources using the luminosity functions of ‘young’ and ‘old’ objects. It is shown that if GPS sources are increasing in radio power with time, it would result in a relatively flatter slope of their luminosity function compared to that of large size radio sources which decrease in radio power.

A simple model was developed in which a radio source, embedded in a King profile medium, evolves in a self similar way under the equipartition energy assumption. This model indeed results in the suggested increase in luminos-

ity for young radio sources, and decrease in luminosity for old, extended objects. The calculated luminosity function for large size radio sources shows a break and slopes at low and high luminosity comparable to that derived by Dunlop & Peacock (1990) for steep spectrum sources. The local luminosity function (LLF) of GPS sources can not be measured directly since so few GPS sources are found at low redshift. Therefore, the knowledge of the cosmological evolution of the luminosity function of steep spectrum sources, as derived by Dunlop & Peacock (1990), is used, so that the LLF can be derived from the complete samples of bright and faint GPS sources. It is shown that this LLF is as expected for radio sources which increase in luminosity with time, which is confirmed by simulations of the young radio source population. Note however, that the bright and faint GPS samples are constructed in very different ways and that therefore large corrections had to be made. Uncertainties are still very large and ideally large samples of GPS sources should be constructed which are uniformly selected at low and high flux densities.

5 ACKNOWLEDGEMENTS

We like to thank the anonymous referee for carefully reading the manuscript and valuable suggestions. We also thank Christian Kaiser and Jane Dennett-Thorpe for helpful comments. This research was in part funded by the European Commission under contracts ERBFMRX-CT96-0034 (CERES) and ERBFMRX-CT96-086 (Formation and Evolution of Galaxies), and SCI-CT91-0718 (The Most Distant Galaxies).*

REFERENCES

- Baldwin J., 1982, In: Extragalactic radio sources, NM, D. Reidel Publishing Co., 1982, p. 21
 Baum S.A., O’Dea C.P., Murphy D.W., de Bruyn A.G., 1990, A&A, 232, 19
 Begelman M.C., 1996, in proceedings of “Cygnus A: A study of a radio galaxy”, eds. C. Carilli & D. Harris (Cambridge, Cambridge University Press), p.209
 Bicknell, G.V., Dopita M.A., O’Dea C.P., 1997, ApJ, 485, 112
 Blake G.M., 1970, ApJ, 6, L201
 Blundell K.M., Rawlings S., Willott C.J., 1999 Astronomical Journal, 117, 677
 van Breugel, W., Miley, G.K., Heckman T., 1984, AJ, 89, 5
 Bondi M., Garrett M.A., Gurvits L.I., 1998, MNRAS, 297, 559
 Dallacasa D., Fanti C., Fanti R., Schilizzi R.T., Spencer R.E., 1995 A&A, 295, 27
 Dallacasa D., Bondi M., Alef W., Mantovani F., 1998, A&AS, 129, 219
 Dunlop J.S., Peacock J.A., 1990, MNRAS, 247, 19
 Fanti R., Fanti C., Schilizzi R.T., Spencer R.E., Nan Rendong, Parma P., Van Breugel W.J.M., Venturi T., 1990, A&A, 231, 333
 Fanti C., Fanti R., Dallacasa D., Schilizzi R.T., Spencer R.E., Stanghellini C., 1995, A&A, 302, 317
 Gregory P.C., Condon J.J., 1991, ApJS, 75 1011
 Hodges M.W., Mutel R.L., Phillips R.B., 1984, AJ, 89, 1327
 Jones T.W., O’Dell S.L., Stein W.A., 1974, ApJ, 192, 261
 Kaiser C.R., Alexander P., 1997, MNRAS, 286, 215
 Kellerman K.I., Pauliny-Toth I.I.K., 1981, ARA&A, 19, 373

- Kühr H., Witzel A., Pauliny-toth I.I.K., Nauber U., 1981, *A&AS*, 45, 367
- Kuncic Z., Bicknell G.V., Dopita M.A., 1998, *ApJ*, 495, L35
- Leahy J.P., Williams A.G., 1984, *MNRAS*, 210, 929
- Murgia M., Fanti C., Fanti R., Gregorini L., Klein U., Mack K-H., Vigotti M., 1999, *A&A*, 345, 769
- Mutel R.L., Hodges M.W., Phillips R.B., 1985, *ApJ*, 290, 86
- O'Dea C.P., Baum S.A., Stanghellini C., 1991, *ApJ*, 380, 66
- O'Dea C.P., Stanghellini C., Baum S.A., Charlot S., *ApJ*, 470, 806
- O'Dea C.P., Baum S.A., 1997, *AJ*, 113, 148
- O'Dea C.P., 1998, *PASP*, 110, 493
- Owsianik I., Conway J.E., 1998, *A&A*, 337, 69
- Owsianik I., Conway, J.E., Polatidis, A.G., 1998, *A&A*, 336, L37
- Peacock J.A., Wall J.V., 1982, *MNRAS*, 198, 843
- Readhead A.C.S, Xu W., Pearson T.J., 1994, in *Compact Extragalactic Radio Sources*, eds Zensus & Kellerman, p19
- Readhead A.C.S., Taylor G.B., Xu W., Pearson T.J., Wilkinson P.N., 1996, *ApJ*, 460, 634
- Rengelink R.B., Tang Y., de Bruyn A.G., Miley G.K., Bremer M.N., Röttgering H.J.A., Bremer M.A.R., 1997, *A&AS*, 124, 259
- Richstone D., Ajhar E.A., Bender R., Bower G., Dressler A., Faber S.M., Filippenko A.V., Gebhardt K., Green R., Ho L.C., Kormendy J., Lauer T.R., Magorrian J., Tremaine S., 1998, *Nature*, 395, 14
- Schoenmakers, A., 1999, PhD thesis, Leiden University
- Scott M.A., readhead A.C.S., 1977, *MNRAS*, 180, 539
- Shklovsky, I. S., 1963, *SvA*, 6, 465
- Shklovsky I.S., 1965, *Nature*, 206, 176
- Snellen I.A.G., Bremer M.N., Schilizzi R.T., Miley G.K., van Ojik R., 1996, *MNRAS*, 279, 1294
- Snellen I.A.G., Schilizzi R.T., de Bruyn A.G., Miley G.K., Rengelink R.B., Röttgering H.J.A., Bremer, M.N., 1998a, *A&AS*, 131, 435
- Snellen I.A.G., Schilizzi R.T., Bremer M.N., de Bruyn A.G., Miley G.K., Röttgering H.J.A., McMahon R.G., Pérez Fournon I., 1998b, *MNRAS*, 301, 985
- Snellen I.A.G., Schilizzi R.T., Bremer M.N., Miley G.K., de Bruyn A.G., Röttgering H.J.A., 1999, *MNRAS*, 307, 149
- Snellen I.A.G., Schilizzi R.T., van Langevelde H.J., 1999b, *MNRAS*, submitted (companion paper)
- Spencer R.E., McDowell J.C., Charlesworth M., Fanti C., Parma P., Peacock J.A., 1989, 240, 657
- Stanghellini C., O'Dea C.P., Baum S.A., Dallacasa D., Fanti R., Fanti C., 1997a, *A&A*, 325, 943
- Stanghellini C., Bondi M., Dallacasa D., O'Dea C.P., Baum S.A., Fanti R., Fanti C., 1997b, *A&A* 318, 376
- Stanghellini C., O'Dea, C. P., Dallacasa, D., Baum, S.A., Fanti, R., Fanti, C., 1998, *A&AS*, 131, 303
- Stanghellini C., O'Dea C.P., Murphy D.W., 1999, *A&AS*, 134, 309
- Subrahmanyan R., Saripalli L., Hunstead R.D., *MNRAS* 279, 257
- Taylor G.B., Readhead A.C.S., Pearson T.J., 1996, *ApJ*, 463, 95
- Trinchieri G., Fabbiano G., Canizares C.R., 1986, *ApJ*, 310, 637
- Tschager W., Schilizzi R.T., Röttgering H.J.A., Snellen I.A.G., Miley G.K., 2000, *A&A* submitted
- Wilkinson P.N., Polatidis A.G., Readhead A.C.S., Xu W., Pearson T.J., 1994, *ApJ*, 432, L87